Drag Model for Coupled CFD-DEM Simulations of Non-spherical Particles

Rolf Lohse and Ulrich Palzer

Abstract The production and handling of non-spherical granular products plays an important role in many industries. It is often necessary to consider the real particle shape of the real particles as an essential prerequisite for modeling these processes reliably. This work presents a new approach for approximating the drag coefficient of non-spherical particles during simulation. This is based on the representation of the particle shape as a clump of multiple spheres, as it is often used in the Discrete Element Method (DEM). The paper describes the calculation of the drag coefficient based on the arrangement of the spheres within the clump depending on the Reynolds number and the flow direction. Numerical simulations of the flow around regularly- and irregularly shaped particles, as well as experiments in a wind tunnel, are used as the basis of model development. The new drag model is able to describe the drag coefficient for irregularly shaped particles within a wide range of Reynolds numbers. It has been implemented in the toolbox CFDEM® coupling. The new drag model is tested within CFD-DEM simulations of particle behavior in a spouted bed.

1 Introduction

Particle-laden multiphase flows are relevant in various areas of process technology. Typical examples are fluidized or spouted beds, pneumatic conveying of granular media and mixing and separation processes. The accurate prediction of the physical behavior of the particles and the continuous fluid phase is important for the three-dimensional modeling of these processes. At higher particle volume concentrations, the interactions among the particles and between the fluid and dispersed phase become more decisive. Also, the shape of the particles has an essential influence on the

R. Lohse (✉)
Weimar Institute of Applied Construction Research,
Über der Nonnenwiese 1, 99428 Weimar, Germany
e-mail: r.lohse@iab-weimar.de

U. Palzer
e-mail: u.palzer@iab-weimar.de

J. M. Nóbrega and H. Jasak (eds.), *OpenFOAM®*,
https://doi.org/10.1007/978-3-319-60846-4_9

particle behavior. For this reason, the simulation with a coupling of the Discrete Element Method (DEM) and CFD methods is the preferred choice, if the computational expense is justified.

2 Modeling of Non-spherical Particles

The shape of a non-spherical particle is often characterized by its sphericity, which is the ratio between the surface of a volume-equivalent sphere and the surface of the real particle. This method is used in many drag models [1, 2]. Other possibilities are the Corey shape factor used by Swamee et al. [3] and the lengthwise and crosswise sphericity used by Leith [4] and Hölzer et al. [5].

In common DEM software (EDEM [6], PFC [7]), a multi-sphere approach is used to model non-spherical particles for bulk mechanics, wherein an arbitrarily shaped particle is approximated by a clump of different spheres (Fig. 1). In the presented work, this multi-sphere arrangement is also used to calculate the drag forces of the particles resulting from the fluid flow in CFD-DEM simulations. Thus, for every sphere within the clump, a partial drag force $F_{D,i}$ is calculated based on the position of the sphere within the clump, the overlap with other particles and the flow direction. The sum of these values over all spheres within a clump gives the drag force of the non-spherical particles F_D, which depends on the orientation of the particle to the fluid flow and the Reynolds number.

2.1 *Drag Forces on Non-spherical Particles*

There are many studies on the drag force coefficient of spheres and non-spherical particles. These include experimental investigations based on settling experiments and wind tunnel tests [8–10]. The influence of the alignment of the particle to the flow is not studied in detail. It is only distinguished in a lengthwise or crosswise flow. Numerical investigations are available for selected particle shapes. Ellipsoids and discs are studied in [11–13], which also include the influence of the angle of

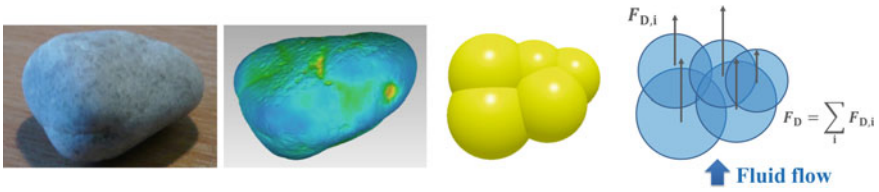

Fig. 1 Transition from a real particle over a 3D scan model to a multi-sphere clump in DEM to the approximation used for the calculation of the drag forces of a non-spherical particle

attack. There are some reliable correlations for the drag coefficient of shaped particles [1–3, 14], which contains the Reynolds number and the sphericity as parameters. Newer formulations by Hölzer and Sommerfeld [5] also capture the influence of the alignment of the particle to the flow. This is done through the usage of the lengthwise and crosswise sphericity of the particles. In the present work, the influence of the particle shape, the Reynolds number and the angle of attack is studied within a wider range. The data from the literature were supplemented with additional CFD calculations and experimental investigation. The approach used is explained below.

2.1.1 Numerical Investigations

Computational fluid dynamics (CFD) is used to calculate the drag of non-spherical particles. The investigations are carried out based on steady state and transient simulations on a stationary particle, with the exact particle shape in an incompressible, turbulent air flow. The SST k–ω model is used for the modeling of the turbulence. The CFD toolbox OpenFOAM® 2.3.x [15] is used to solve the Reynolds-averaged Navier–Stokes (RANS) equation for the flow around the investigated particle shapes, which are shown in Fig. 2. These include both regularly shaped particles, such as cylinders and ellipsoids, and irregularly shaped particles, which were obtained through a 3D scanner. First, simulations for the flow around a sphere were used to validate the computational model. It was found that the drag forces were calculated in good

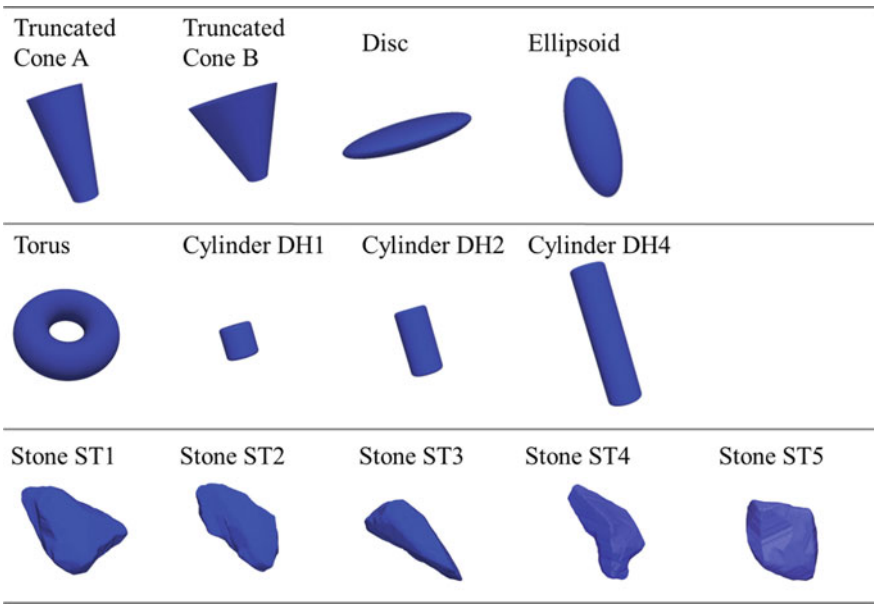

Fig. 2 Overview of the investigated particle shapes

accordance with the known models from the literature [16, 17] up to a Reynolds number of about 14,000. For the simulation of the flow around the arbitrarily shaped particle, the numerical investigations are carried out for Reynolds numbers ranging from 1 to 5000.

2.1.2 Experimental Investigations

A wind tunnel was used for experimental studies of the drag force on non-spherical particles. This Göttinger-Type wind tunnel, build by Westenberg Engineering, has a rectangular-shaped nozzle of 300 × 300 mm and an open test section of 600 mm length (Fig. 3). The possible air velocities are between 0.5 and 40 m/s. The alignment of the particle to the flow can be defined by the mounting device, which is connected to a six-axis force sensor so as to measure the drag force onto the investigated object. The validation of the measurement device was performed with different-sized spheres at the full velocity range of the wind tunnel. Further trials with ellipsoids showed that a minimal air velocity of 8 m/s was sufficient for the investigated particle sizes to ensure a good reproducibility and accuracy of the measurements.

The experiments were performed for selected particle shapes from Fig. 2. This involved truncated cone A, an ellipsoid and different cylinders. The particles were produced with a 3D printer, wherein an adapter for the connection with the measuring device was integrated. The study with the wind tunnel included 80 measurement series of five–eight variants of the particle Reynolds number. The drag forces were measured at flow rates from 5 to 35 m/s. The resulting particle Reynolds numbers were between 15,000 and 40,000. The angle of attack was changed stepwise with ϕ = 0, 30, 45, 75 and 90° (ellipsoid, cylinder) and ϕ = 0, 45, 90, 135 and 180° (truncated cone).

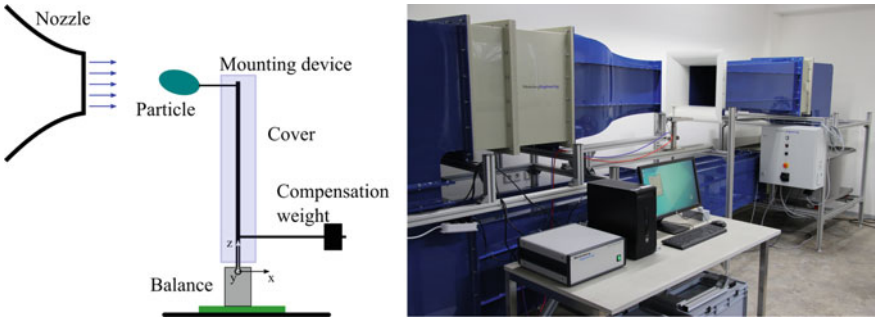

Fig. 3 Schematic of the measurement arrangement (left) and closed wind tunnel test facility (right)

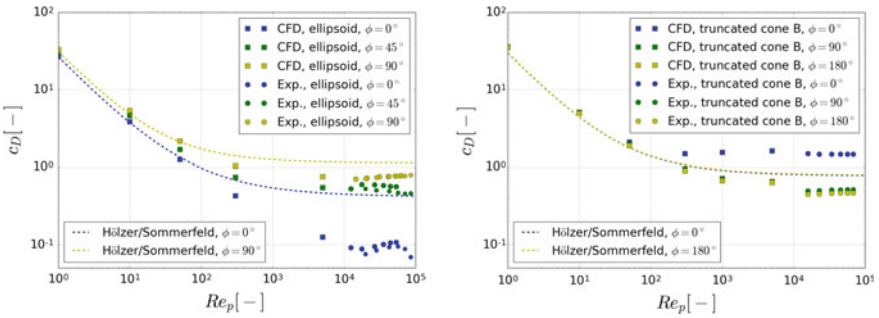

Fig. 4 Results of the numerical simulations and wind tunnel test for the drag coefficient of the ellipsoid (left) and the truncated cone (right) for different angles of attack and Reynolds numbers

2.1.3 Results

The results of the investigation from the wind tunnel tests and the numerical simulation are shown in Fig. 4. In addition, the data are compared with the drag model by Hölzer and Sommerfeld [5]. It can be seen that the numerical simulations fit well with the experimental results for the ellipsoid. Both sets of data are below the model by Hölzer and Sommerfeld, especially at higher Reynolds numbers. The results of the simulation and the experiments show a small jump for the truncated cone around $Re = 10{,}000$. It has not yet been fully clarified as to whether the reason is to be found in the measurement or in the simulation approach.

The simulation and the experimental data for the truncated cone show a clear influence of the angle of attack on the drag coefficient. This behavior cannot be reproduced by the drag model by Hölzer and Sommerfeld. There is no difference shown between the alignment to the flow for 0° and 180°. It can be recognized from the wind tunnel tests that the drag coefficient is nearly independent of the flow velocity for the investigated Reynolds numbers above 10,000. The known drag models from the literature confirm this behavior. Only the particle shape and the angle of attack influence the drag coefficient value.

3 Drag Model Development

The non-spherical particle shape is represented by a clump of multiple spheres. The spheres can have different diameters and can overlap each other. The idea of this model approach is to estimate the drag coefficient in two steps. First, the acting drag force for each sphere within the clump is approximated in dependence on the flow direction, position, overlapping and shading of each sphere. With the sum of the drag forces on each sphere, the drag coefficient $c_{D,S}$ can be determined for the particle. In the literature, many models exist for the drag of single spheres. Morrison's model

[16] covers a very wide range of Reynolds numbers and is used as the basis for the new drag model.

$$c_{D,S} = \frac{24}{Re_S} + \frac{2.6\left(\frac{Re_S}{5.0}\right)}{1+\left(\frac{Re_S}{5.0}\right)^{1.52}} + \frac{0.411\left(\frac{Re_S}{263000}\right)^{-7.94}}{1+\left(\frac{Re_S}{263000}\right)^{-8.00}} + \frac{{Re_S}^{0.80}}{461000}\,. \tag{1}$$

A sphere Reynolds number is calculated for each sphere within the clump in dependence on the diameter and the relative velocity between particle and fluid flow. The drag force of the sphere $F_{D,S}$ is calculated including a weight factor W

$$F_{D,S} = W\frac{c_{D,S}\,\rho}{2}{U_{rel}}^2\frac{\pi}{4}{d_S}^2, \tag{2}$$

where U_{rel} is the local relative velocity, d_S the diameter of the sphere and ρ the fluid density. With the sum of the drag forces of all spheres, the drag coefficient of the particle c_D can be determined

$$c_D = \frac{\sum F_{D,S}}{\frac{\rho}{2}{U_{rel}}^2\frac{\pi}{4}{d_V}^2}\,, \tag{3}$$

where d_V is the diameter of the volume-equivalent sphere. The weighting factor W has to be defined as a function of the position of the sphere within the clump, the influence of the particle Reynolds number and the alignment of the clump to the flow. Different combinations of several parameters that describe the position and the size of the spheres inside the clump are investigated for the definition of the weighting factor. Some examples of these parameters are listed below and explained in more detail in Fig. 5.

- Volume of a sphere, which is not overlapped by another sphere
- Relative free surface a_{fs}, which is the ratio of the surface area, having direct contact with the surrounding fluid A_{fs} and sphere surface A_S ($a_{fs} = A_{fs}/A_S$)
- Incident flow surface ratio of the sphere ($a_{sh} = A_{sh}/A_S$)
- Incident flow surface ratio of the sphere with reversed flow direction ($a_{bs} = A_{bs}/A_S$)
- Diameter of a sphere d_S
- Distance to the leading sphere s (parallel to the flow vector).

Different functional combinations from these parameters were examined for the weighting factor, including the sphere Reynolds number. The best variant so far is given by

$$W = A\ {Re_S}^B\left(C\ {a_{sh}}^D + E\ {a_{bs}}^F\right) + G\ {Re_S}^H e^{\left(I\ {a_{sh}}^J + K\ {a_{bs}}^L\right)} + M\ {Re_S}^N\left(O\ {a_{fs}}^P\right), \tag{4}$$

with A to P as model coefficients.

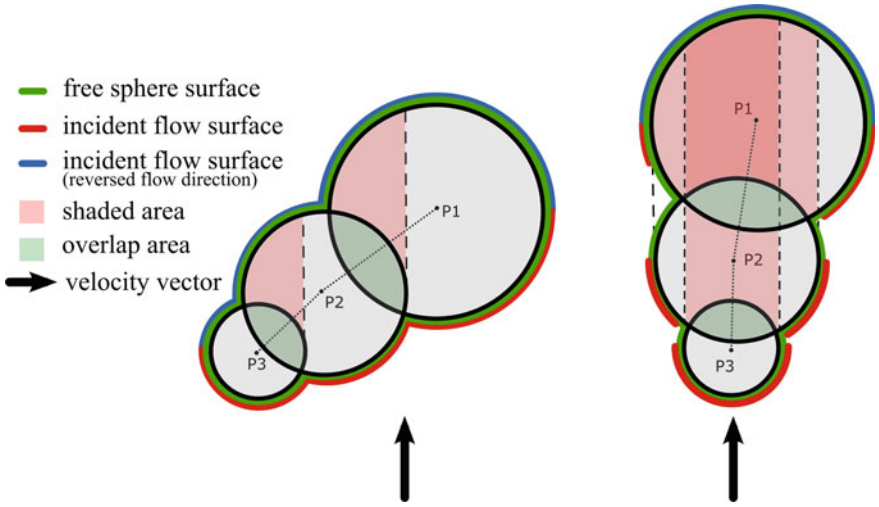

Fig. 5 Visualization of the parameters for the calculation of the weighting factor W

The values of the coefficients contained in the model functions for the weighting factor were determined using a fitting algorithm. The definition is based on the results of CFD simulations for selected particle shapes. These particles were discretized by a clump of spheres with various sphere numbers. The weighting factor is determined by Eq. 4 for each of these spheres and the appropriate drag coefficient is calculated by Eq. 3. The coefficients in Eq. 4 are adjusted to fit best the values from the CFD calculation for a wide range of Reynolds numbers and angles of attack by an optimization algorithm. Thereby, a particle swarm approach is used. The problem is implemented in combination with the python program deap [18], which processes the optimization on a multi-processor platform in parallel.

The coefficients used in Eq. 4 are listed in Table 1. The resulting drag coefficient for a truncated cone and an irregularly shaped particle are shown in Fig. 6 in dependence on the Reynolds number and the angle of attack. The new drag model gives a better agreement with the CFD results in comparison to the model by Hölzer and Sommerfeld.

Table 1 Shape-independent parameters used for calculation of the weighting factor in Eq. 4

Parameter	Value	Parameter	Value	Parameter	Value	Parameter	Value
A	0.272444	E	0.860548	I	2.993242	M	1.689610
B	0.179754	F	0.711180	J	2.077819	N	0.127088
C	−0.380534	G	0.034872	K	0.216286	O	−0.004679
D	5.650548	H	−0.021070	L	0.256386	P	−0.097940

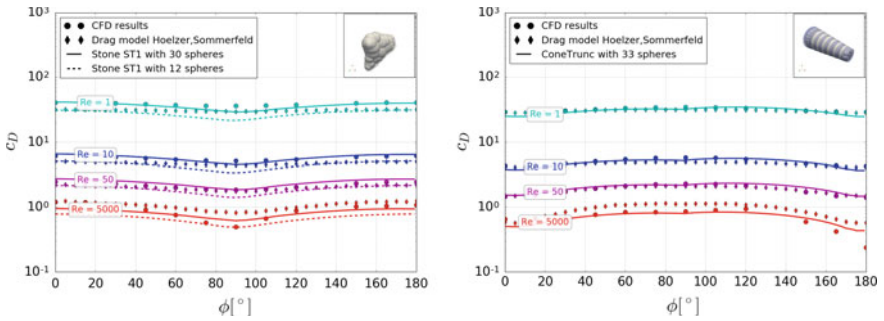

Fig. 6 Drag coefficient for the new model depending on the Reynolds number and particle orientation in comparison to CFD data and the drag model by Hölzer and Sommerfeld [5]; truncated cone (left) and stone ST1 (right)

4 Application

The new drag model will be tested on a complex flow configuration. Therefore, experimental investigations on a spouted bed configuration are processed. The toolbox CFDEM® coupling is used to calculate the behavior of the fluid and the granular phase. This is done through a coupling of the CFD code OpenFOAM® [15] and the DEM code LIGGGHTS [19]. The momentum conservation equation for the fluid phase uses the incompressible formulations according to a pressure gradient force model (PGF or model A [20, 21]) that is implemented in CFDEM® coupling as follows:

$$\frac{\partial \varepsilon_f U_i}{\partial t} + \frac{\partial \varepsilon_f U_i U_j}{\partial x_i} = -\varepsilon_f \frac{\partial p}{\partial x_i} + \frac{\partial \varepsilon_f \tau}{\partial x_i} + \varepsilon_f g - F_{pf}, \tag{5}$$

where ε_f is the fluid phase fraction, U the fluid velocity, τ the shear tensor, and F_{pf} the sum of the volume forces for the coupling between the fluid and the granular phase. The simulations are performed with the cfdemSolverPiso solver of CFDEM® coupling [19] using a four-way coupling approach that considers the particle–particle and particle–fluid interactions. The new drag model is valid for the flow around a single particle. In order to take into account effects resulting from locally high particle volume concentrations (swarm effects), the drag model is combined with a correlation by DiFelice [22]. This approach was also used by Hilton et al. [23] and Oschmann et al. [24]. The drag force F_D also depends on the local particle volume concentration ε_f and the model parameters χ

$$F_D = \frac{c_D \rho}{2} U^2 \frac{\pi}{4} {d_V}^2 {\varepsilon_f}^{(1-\chi)}, \tag{6}$$

where

$$\chi = 3.7 - 0.65 exp\left(-\frac{(1.5 - log(Re))^2}{2}\right). \tag{7}$$

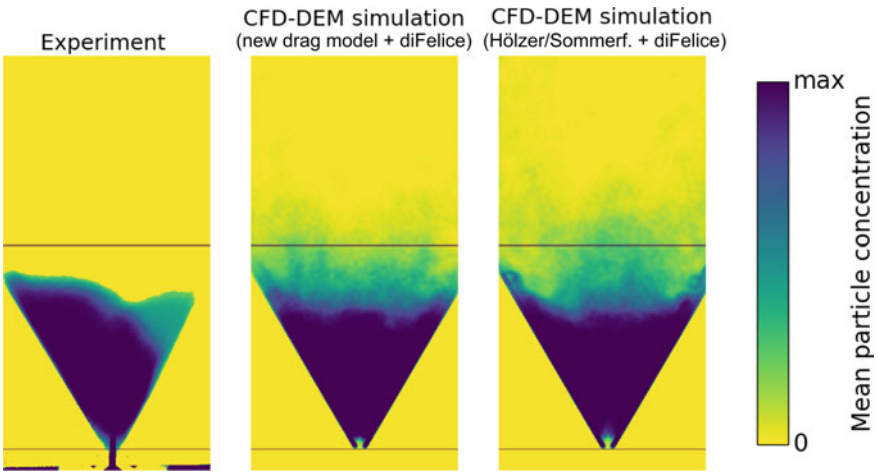

Fig. 7 Mean particle distribution within the spouted bed for the experimental and numerical investigations with 1000 tori: experiments (left), CFD-DEM calculation with the new drag model (middle) and the drag model by Hölzer and Sommerfeld [5] (right)

The combination with DiFelice's approach was implemented and tested, both for the newly developed drag model and the drag model by Hölzer and Sommerfeld. The grid resolution for spouted bed geometry was chosen such that the flow field is still well-discretized and most grid cells are larger than the diameter of the Clump spheres. In the area of the wall and the inlet region, the cell size is much smaller than the spheres used. So, the local particle concentration may not be calculated correctly in these regions. A resolved CFD-DEM method presented in [25] could lead to better results, but requires higher computational costs and was not tested within this work. The simulation was performed for a real time of 30 s.

The experimental setup uses a camera in combination with a backlight to describe the particle behavior. A time series of 300 images over 5 min is used to determine the average bed dimension. The results of the simulations for the motion of tori in the spouted bed are shown in Fig. 7. All performed CFD-DEM simulations show a similar fluidization of particles compared to the experiment. The average calculated bed height is similar to the experiments. The particle velocities close to the walls are higher, so that particles in this region are transported well above the average bed height, a phenomenon that has not been observed experimentally. The differences between experiments and simulations in the inlet region are due to the experimental setup, whereas this region was not sufficiently well-lit.

There are only minor differences between the results with the new drag model and those with the model by Hölzer and Sommerfeld. However, the whirling up of a few particles at the wall is more pronounced with the model by Hölzer and Sommerfeld. The results with the new drag model show a slightly better agreement with the experimental results.

5 Conclusions

A new model is presented to approximate the drag coefficient of non-spherical particles using a clump of multiple spheres to represent the shape of the particle. Numerical simulation and wind tunnel experiments are performed to determine the drag forces of regularly and irregularly shaped particles for a wide range of Reynolds numbers and particle orientations. These data are used to determine the necessary model parameters. The drag model shows a good fit with the CFD results within a wide range of particle shapes, Reynolds numbers and particle orientations. It gives, in some cases, better results than the widely used model by Hölzer and Sommerfeld [5]. The new drag model is implemented within the CFDEM® coupling environment. It is used in combination with the correlation by DiFelice [22] to capture the influence of high particle concentrations on the drag values. The application of the drag model for the simulation of non-spherical particles in spouted beds by means of CFD-DEM calculations gives a good agreement with experimental results.

Acknowledgements This work was funded by the German Federal Ministry of Economy and Technology (BMWi) in the framework of the INNO-KOM-Ost project under grant VF130034.

References

1. Haider, A., Levenspiel, O.: Drag coefficient and terminal velocity of spherical and nonspherical particles. Powder Technology **58**, 63–70, (1989)
2. Loth, E.: Drag of non-spherical solid particles of regular and irregular shape. Powder Technology **182**, 342–353, (2008)
3. Swamee, P., Ojha, C.: Drag Coefficient and Fall Velocity of nonspherical particles. Journal of Hydraulic Engineering **117**, 660–667, (1991)
4. Leith, D.: Drag on Nonspherical Objects. Aerosol Science and Technology **6**, 153–161, (1987)
5. Hölzer, A., Sommerfeld, M.: New simple correlation formula for the drag coefficient of non-spherical particles. Powder Technology **184**, 361–365, (2008)
6. DEM-Solutions, EDEM version 2.7, Edinburgh (2015)
7. Itasca Consultings GmbH, PFC3D version 4.0, Gelsenkirchen, (2015)
8. Becker, H.: The Effects of Shape and Reynolds Number on Drag in the Motion of a Freely Oriented Body in an Infinite Fluid. Can. J. Chem. Eng. **37**, 85–91, (1959)
9. Kasper, G., Niida, T., Yang, M.: Measurements of Viscous Drag on Cylinders and Chains of Spheres with Aspect Ratios Between 2 and 50. Journal of Aerosol Science **16**, 535–556, (1985)
10. Pettyjohn, E. S., Christiansen, E. B.: Effect of Particle Shape on Free-Settling Rates of Isometric Particles. Chemical Engineering Progress **44**, 157–172, (1948)
11. Dwyer, H. A., Dandy, D. S.: Some influences of particle shape on drag and heat transfer. Physics of Fluids A: Fluid Dynamics **2**, 2110–2118, (1990)
12. Hölzer, A.: Bestimmung des Widerstandes, Auftriebs und Drehmoments und Simulation der Bewegung nichtsphrischer Partikel in laminaren und turbulenten Strmungen mit dem Lattice-Boltzmann-Verfahren. Martin-Luther-Universitt Halle-Wittenberg, 2007
13. Zastawny, M., Mallouppas, G., Zhao, F., van Wachem, B.: Derivation of drag and lift force and torque coefficients for non-spherical particles in flows. International Journal of Mineral Processing **39**, 227–239, (2012)
14. Ganser, G. H.: A rational approach to drag prediction of spherical and nonspherical particles. Powder Technology **77**, 143–152, (1993)

15. OpenCFD Ltd. (ESI-Group), OpenFOAM® version 2.3, Bracknell, UK (2014)
16. Morrison, F. A.: Data Correlation for Drag Coefficient for Sphere. Department of Chemical Engineering, Michigan Technological University, Houghton, MI (2013) Available via http://www.chem.mtu.edu/~fmorriso/DataCorrelationForSphereDrag2013.pdf
17. Schiller, L., Naumann, A.: Über die grundlegenden Berechnungen bei der Schwerkraftaufbereitung. Zeitschrift Verein Deutscher Ingenieure **77**, 318–320, (1933)
18. Fortin, F.-A., De Rainville, F.-M., Gardner, M.-A., Parizeau, M., Gagn, C.: DEAP: Evolutionary Algorithms Made Easy. Journal of Machine Learning Research **13**, 2171–2175, (2012)
19. Goniva, C., Kloss, C., Deen, N., Kuipers, J., Pirker, S.: Influence of Rolling Friction Modelling on Single Spout Fluidized Bed Simulations. Particuology **5**, 582–591, (2012)
20. Kafui, K. D., Thornton, C., Adams, M. J: Reply to comments by Feng and Yu on "Discrete particle-continuum fluid modelling of gas-solid fluidised beds" by Kafui et al. Chemical Engineering Science **59**, 719–722, (2004)
21. Zhou, Z. Y., Kuang, S. B., Chu, K. W., Yu, A. B.: Discrete particle simulation of particle–fluid flow: model formulations and their applicability. Journal of Fluid Mechanics **661**, 482–510, (2010)
22. Di Felice, R.: The voidage function for fluid–particle interaction systems. International Journal of Multiphase Flow **20**, 153–159, (1994)
23. Hilton, J., Cleary, P. (2009) The Role of Particle Shape in Pneumatic Conveying. In: Proceedings of the Seventh International Conference on CFD in the Minerals and Process Industries (CSIRO)
24. Oschmann, T., Vollmari, K., Kruggel-Emden, H., Wirtz, S.: Numerical investigation of the mixing of non-spherical particles in fluidized beds and during pneumatic conveying. Procedia Engineering **102**, 976–985, (2015)
25. Hager, A., Kloss, K., Pirker, S., Goniva, C. (2012) Parallel Open Source CFD-DEM for Resolved Particle-Fluid Interaction. In: Proceedings of the Ninth International Conference on CFD in the Minerals and Process Industries (CSIRO)